

To appear in the Dec 2000 issue of the Astronomical Journal

Dynamical Constraints on the Formation of NGC 4472 and Its Globular Clusters

Stephen E. Zepf

Department of Astronomy, Yale University, New Haven, CT 06520;
 zepf@astro.yale.edu

Michael A. Beasley¹

Department of Physics, University of Durham, South Road, Durham DH1 3LE, England;
 m.a.beasley@durham.ac.uk

Terry J. Bridges¹

Anglo-Australian Observatory, Epping, NSW, 1710, Australia; tjb@aaopep.aoa.gov.au

David A. Hanes¹

Department of Physics, Queen's University, Kingston, ON K7L 3N6, Canada;
 hanes@astro.queensu.ca

Ray M. Sharples¹

Department of Physics, University of Durham, South Road, Durham DH1 3LE, England;
 r.m.sharples@durham.ac.uk

Keith M. Ashman

Department of Physics and Astronomy, University of Kansas, Lawrence, KS 66045;
 ashman@kusphy.phsx.ukans.edu

Doug Geisler

Grupo de Astronomia, Universidad de Concepción, Casilla 160-C, Concepción, Chile;
 doug@kukita.cfm.udec.cl

ABSTRACT

We present new radial velocities for 87 globular clusters around the elliptical galaxy NGC 4472, and combine these with our previously published data to create a data set of velocities for 144 globular clusters around NGC 4472. We utilize this data set to analyze the kinematics of the NGC 4472 globular cluster system. The new

¹Visiting Astronomers, Canada-France-Hawaii Telescope, which is operated by the National Research Council of Canada, the Centre National de la Recherche Scientifique, and the University of Hawaii.

data confirms our previous discovery that the metal-poor clusters have significantly higher velocity dispersion than the metal-rich clusters in NGC 4472. We also find very little or no rotation in the more spatially concentrated metal-rich population, with a resulting upper limit for this population of $(v/\sigma)_{proj} < 0.34$ at a 99% confidence level. The very small angular momentum in the metal-rich population requires efficient angular momentum transport during the formation of this population which is spatially concentrated and chemically enriched. Such angular momentum transfer can be provided by galaxy mergers, but has not been achieved in other extant models of elliptical galaxy formation that include dark matter halos. We also calculate the velocity dispersion as a function of radius, and show that it is consistent with roughly isotropic orbits for the clusters and the mass distribution of NGC 4472 inferred from X-ray observations of the hot gas around the galaxy.

Subject headings: dark matter — galaxies: formation — galaxies: halos — galaxies: individual (NGC 4472) — galaxies: kinematics and dynamics — galaxies: star clusters

1. Introduction

Although early-type galaxies make up much of the stellar mass in the local universe (e.g. Fukugita, Peebles, & Hogan 1998, Coppi & Zepf 2000), there is no consensus on when or how they formed. The possibilities range from monolithic collapse at high redshift to formation via galaxy mergers over a range of redshifts. Many of the integrated properties of elliptical galaxies can be accounted for by both scenarios, making it difficult to determine the formation histories of these galaxies. For example, one of the salient observational features of the population of early-type galaxies is that their color-magnitude and $Mg_2 - \sigma$ relations have small scatter. However, both early collapse models (e.g. Kodama & Arimoto 1997) and hierarchical merging models (e.g. Kauffmann & Charlot 1998) have been shown to be consistent with the observed correlations. Both mergers and collapse models can also be made consistent with current observations of galaxies at high redshift. The small number of very red galaxies in deep K-selected samples indicates that most ellipticals formed some of their stars at $z \lesssim 3$ (Treu & Stiavelli 1999, Barger et al. 1999, Zepf 1997), with a few exceptions (e.g. Treu et al. 1998, Benitez et al. 1999). However, this only requires that some of the formation activity of ellipticals take place at lower redshifts, and does not explicitly favor one model or another.

A critical observation that must be addressed by any successful model of galaxy formation is the weak or absent stellar rotation in giant ellipticals. In contrast to the dynamical insignificance of rotation in elliptical galaxies, the dynamics of spiral galaxies are dominated by rotation, resulting in about an order of magnitude more total angular momentum for spirals compared to the visible components of ellipticals (e.g. Silk & Wyse 1993). The large difference in angular momentum between elliptical and spiral galaxies has long been recognized as one of the most fundamental

problems in galaxy formation. Moreover, this difference between the angular momenta of spiral and elliptical galaxies is not expected to be true of their dark matter halos. All extant theoretical models predict that the spin-up of galactic halos through tidal torques will be similar for all galaxies, so the range of halo angular momenta is smaller than the observed difference between elliptical and spiral galaxies (e.g. Heavens & Peacock 1988, Barnes & Efstathiou 1987, Warren et al. 1992, Eisenstein & Loeb 1995). In terms of the commonly used dimensionless spin parameter $\lambda = LE^{1/2}/GM^{5/2}$, where L is the angular momentum E is the energy, and M is the mass, all halos have $\lambda \simeq 0.06$. These calculations also find that the angular momentum of a halo is mostly independent of its mass or environment, so any differences between the angular momentum of elliptical and spiral galaxies can not be accounted for solely by their different masses or environments.

The rotation and density of spiral galaxies can be straightforwardly understood as the result of the collapse and spin-up of baryonic material inside a dark matter halo (e.g. Fall & Efstathiou 1980). More specifically, for a protogalaxy with $\lambda \sim 0.06$, a collapse factor of roughly ten produces both the observed rotation and the density of spiral disks. However, there is no such simple explanation for the low angular momentum in the visible parts of elliptical galaxies. As described above, calculations of the tidal torques on galaxy halos show that all halos have fairly similar specific angular momentum. Moreover, the similar stellar densities of ellipticals and spirals suggest that the gas in each galaxy type collapsed by roughly the same degree during the galaxy formation process. The comparable dark matter contributions within the visible regions of each galaxy type, as well as the extended nature of dark matter halos around both spirals and ellipticals, also imply that the gas collapse factors in both morphological types must have been similar. Since the collapse factors seem to be similar, and the initial values of λ are expected to be similar, the dramatic difference in the rotation in the visible regions of ellipticals and spirals is a critical constraint on the galaxy formation process. Specifically, spirals and ellipticals must have had different formation processes, with efficient angular momentum transport occurring during the formation of elliptical galaxies.

It has long been realized that galaxy mergers might provide a mechanism for transporting angular momentum out of the visible regions of elliptical galaxies (e.g. Fall 1979, Toomre 1977, Barnes & Hernquist 1992). The hypothesis that elliptical galaxies form from major mergers while spiral galaxies have avoided a major merger in the recent past is therefore an attractive one. However, as described above, it is difficult to demonstrate from observational data that elliptical galaxies today formed from mergers in the past. Some of the strongest evidence that elliptical galaxies form episodically comes from the study of the colors of globular clusters around nearby ellipticals. These studies show that elliptical galaxies often have globular cluster systems with bimodal metallicity distributions (Ashman & Zepf 1998 and references therein, see also Kundu 1999 and Gebhardt & Kissler-Patig 1999). The distinct globular cluster populations observed in many ellipticals suggest episodic formation and are inconsistent with simple monolithic collapse models. In contrast, bimodal globular cluster systems were predicted by Ashman & Zepf (1992)

for elliptical galaxies that formed from mergers of gas-rich spirals. Specifically, Ashman & Zepf (1992) predicted that elliptical galaxies would have a population of metal-poor globulars from the halos of the progenitor spirals, and a population of metal-rich clusters formed in the merger that made the elliptical. Subsequent observations have produced a large body of observational evidence indicating that globular clusters can form in gas-rich mergers (see reviews by Schweizer 1998, Ashman & Zepf 1998, and references therein). Thus both fundamental predictions of the merger model have been supported by subsequent observations - globular clusters are observed to form in mergers and the proposed product of these mergers, elliptical galaxies, show evidence for multiple populations of globular clusters.

The discovery of young globular clusters in mergers and of bimodality in the globular cluster systems of ellipticals were successfully predicted by the merger models. However, for many elliptical galaxies the specific number and inferred metallicity of the blue, metal-poor globular clusters is not in detailed agreement with the predictions of the simple merger model. In the simplest merger picture, these metal-poor clusters come from the halo populations of the progenitor spirals, and therefore the metal-poor population in ellipticals should have the same metallicity and specific frequency (number per stellar luminosity, or preferably, number per stellar mass). However, some elliptical galaxies such as M87 appear to have more metal-poor clusters than can be accounted for by combining the halo populations of spirals like the Galaxy and M31 (e.g. Forbes, Brodie, & Grillmair 1997, Lee, Kim, & Geisler 1998) while other ellipticals such as NGC 3923 (Zepf, Ashman, & Geisler 1995) and IC 4051 (Woodworth & Harris 2000) may either not have a substantial metal-poor globular cluster population or have one which is more metal-rich than the halo populations of the Galaxy and M31. Zepf et al. (1995) and Ashman & Zepf (1998) have noted that, in the context of the merger models, these observations suggest variations in the properties of the globular cluster systems of the progenitor spirals, as well as the possibility of significant accretion of low-metallicity globular clusters and associated dwarf galaxies.

Following the discovery of the bimodality in the globular cluster systems of elliptical galaxies, models were constructed to try to account for bimodality without major mergers. One example is the proposal that elliptical galaxies simply form in two phases, an initial spatially extended phase of metal-poor globular cluster formation followed by the later formation of metal-rich clusters after dissipation and enrichment, with some internal mechanism that turns off globular cluster formation between the two globular cluster formation phases (Forbes et al. 1997, Harris, Harris, & McLaughlin 1998). Alternatively, it has also been proposed that the central component of elliptical galaxies undergoes standard dissipative collapse, and the metal-poor globular cluster population is accreted later (Cote, Marzke, & West 1999).

The key physical element of all models is that angular momentum conservation requires the dissipative collapse that leads to the formation of the metal-rich globular clusters to also result in significant rotation in the metal-rich globular cluster population. The only way to avoid this conclusion is to have a mechanism to efficiently transport angular momentum outwards. Merger models have been shown to provide such a mechanism, while smooth dissipative collapse models do

not naturally transport angular momentum efficiently. Therefore, the kinematics of the globular cluster systems provides a way to test if the physics of the formation of elliptical galaxies and their globular cluster systems is consistent with smooth dissipative collapse or if angular momentum is required to be transported outwards. Moreover, if angular momentum transport is indicated by observations in the inner regions of an elliptical, it might be possible to observe the angular momentum transferred outwards in the kinematics at very large radii, as possibly found for the M87 globular cluster system by Kissler-Patig & Gebhardt (1998) based on the data of Cohen & Ryzhov (1997).

Measurements of the radial velocities of globular clusters also provide information about the mass distribution of the galaxy and the orbits of the clusters. Globular clusters are particularly useful for studying the dynamics of the outer halos of elliptical galaxies because they can be observed out to much larger radii than it is possible to obtain spectroscopy of the integrated light. A very large number of velocities are required to independently determine the mass distribution and the orbits of the tracer particles in a completely non-parametric way (e.g. Merritt & Tremblay 1994). However, if the mass distribution inferred from X-ray observations and the assumption of hydrostatic equilibrium in the hot gas is adopted, the orbits of the globular clusters can be constrained. Conversely, if assumptions are made about the cluster orbits (e.g. that they are isotropic), then the mass distribution can be estimated. In practice, a sensible approach is to check for consistency of the mass distribution determined via the X-ray observations of the hot gas with dynamical measurements given simplifying assumptions about the orbits, as each technique has its own systematic concerns which are mitigated if the independent approaches agree.

In this paper, we present the results of a spectroscopic survey of globular clusters around the Virgo elliptical NGC 4472. We focus on the analysis of the kinematics of the globular cluster system and its implications. A discussion of the ages and metallicities of the NGC 4472 globular clusters is given in Beasley et al. (2000). The observations and data reduction are described in §2. The results of our analysis of these data are presented in §3. In §3.1 we compare the velocity dispersions of the different globular cluster populations, in §3.2 we analyze the rotation of the cluster populations, in §3.3 we study the radial trends in the velocity dispersion and rotation, and in §3.4 we examine the mass distribution of NGC 4472 inferred from our data. The implications of these results are discussed in §4, and our conclusions given in §5.

2. Observations and Data Reduction

We obtained spectra of globular cluster candidates around NGC 4472 using the Multi-Object Spectrograph (hereafter MOS, Crampton et al. 1992, LeFevre et al. 1994) on the Canada-France-Hawaii Telescope over parts of three nights in May 1998. MOS is an effective instrument for this study because its relatively large field of view allows for efficient multiplexing of the NGC 4472 globular cluster system, which extends out to many arcminutes from the center of the galaxy (cf. Rhode & Zepf 2000). The candidate globular clusters were selected from the photometric study of

the NGC 4472 globular cluster system by Geisler et al. (1996). We obtained spectra through four slitmasks, each of which contained slitlets for approximately 45 globular cluster candidates. We preferentially targeted cluster candidates with magnitudes between $19.5 < V < 21.5$, but included fainter clusters when useful for maximizing the number of targets in each mask. About 2/3 of the slitlets yielded useful spectra, with the remainder having either low signal-to-noise or problematic sky subtraction.

The spectra were obtained with a 600 l/mm grism, giving a resolution of 2.2 Å per pixel, and a spectral range of $3800 - 6500\text{\AA}$. The data were processed with flat fields taken at the beginning and end of the night, and wavelength calibrated using frequent Hg arcs. After extraction of the object spectra and sky subtraction, the radial velocities of the candidate globular clusters were determined by cross-correlation (e.g. Tonry & Davis 1979) with six template stars of known velocity and spectral types ranging from F8V to K0III. The ‘r’ value of the cross-correlation was required to be greater than 2.5 for a velocity measurement to be included in our final sample. The final velocity for each object was determined by a weighted average of the velocities returned by the cross-correlation with each of the six template stars, where the weighting was given by the cross-correlation peak height of each template. The data reduction procedures are described more completely in Beasley et al. (2000).

The formal errors returned by the cross-correlation task for each globular cluster are given in Table 1 below. These are typically $50\text{--}100 \text{ km s}^{-1}$. A check on these errors can be made by comparing the velocities for the 13 clusters for which we have velocities from both this analysis and our earlier work (Sharples et al. 1998, hereafter S98). The result is a mean difference of -17 km s^{-1} with an uncertainty in any individual measurement of 78 km s^{-1} . Much of the dispersion is driven by a large offset for one cluster, so the typical uncertainty may be smaller. Regardless, these uncertainties are much smaller than the velocity dispersion of NGC 4472, so the measurement errors in the velocities of individual clusters do not have a significant effect on the results.

3. Results

In Table 1, we list the positions, magnitudes, colors, and radial velocities for the 144 clusters around NGC 4472 for which we have spectra. This table includes 100 new globular cluster velocities obtained in the observations described above, and 57 previously published by us (S98), which also included some from earlier work by Mould et al. (1990). For the 13 clusters with data from both datasets, the tabulated velocity is from the observation with the strongest cross-correlation. These data form the basis for the analysis presented in the remainder of this paper. For completeness, we also list in Table 2 the 20 objects for which we obtained spectra and found them to be foreground stars or background galaxies. Our 83% success rate in spectroscopically confirming our targets as globular clusters is higher than earlier work. This high success rate is likely due to selection of targets from high quality photometry, and bodes well for future spectroscopic programs.

In addition to analyzing the populations as a whole, we also investigate the kinematic properties of the metal-rich and metal-poor populations of globular clusters in NGC 4472. These populations were first identified through the discovery of bimodality in the color distribution of the NGC 4472 globular cluster system (Zepf & Ashman 1993 and many subsequent papers). That these color differences are primarily due to metallicity is now confirmed by spectroscopy (Beasley et al. 2000). Further evidence for metallicity driving the color distribution is provided by analysis of the luminosity functions of the red and blue globular clusters (e.g. Puzia et al. 1999, Lee & Kim 2000). In order to divide our sample into populations of metal-rich and metal-poor clusters, we apply the KMM mixture-modeling algorithm to the full dataset of Geisler et al. (1996). This objective analysis divides the sample at a color of $(C - T_1) = 1.625$. Clusters bluer than this are more likely to belong to the metal-poor population while those redder than this value are more likely to belong to the metal-rich population. This is the same analysis and color cut used in S98. This assignment represents the best statistical estimate of whether a globular cluster belongs to the metal-rich or metal-poor population. However not every cluster will necessarily be assigned to the population to which it truly belongs because of possible overlap in the color distributions of the different cluster populations as well as photometric errors. This will tend to make it more difficult to detect physical differences between the metal-rich and metal-poor cluster populations, particularly for clusters near the boundary.

The full dataset is plotted in Figure 1. This figure shows the distribution on the sky of the globular clusters for which we have velocities, and also includes a rough indication of the velocities of these objects, as well as their identification as a member of the metal-rich or metal-poor cluster population. The bulk of this paper is aimed at a quantitative analysis of the velocities and positions of the clusters presented in Table 1 and Figure 1.

3.1. Velocity Dispersions

One of the goals of this study was to compare the kinematics of the metal-rich and metal-poor globular cluster populations of NGC 4472. In our earlier work with radial velocities for 57 globulars we found tentative evidence (86% confidence level) for a higher velocity dispersion in the metal-poor population compared to the metal-rich population (S98). A difference in velocity dispersions between the metal-rich and metal-poor globular cluster populations is critical evidence that these populations have real physical differences, since the division between the metal-rich and metal-poor cluster populations was made by an objective analysis of the colors alone.

Figure 2 shows the comparison of the velocity distribution of the red, metal-rich clusters, and the blue, metal-poor clusters around NGC 4472. This plot demonstrates that the new, larger dataset strongly confirms our original discovery that the metal-poor cluster population has a significantly higher velocity dispersion than the metal-rich cluster population. Specifically, a F-test indicates that the two populations have a different dispersion at $> 99.9\%$ confidence level. The values of the velocity dispersion in each population are $\sigma = 221 \pm 22 \text{ km s}^{-1}$ for the

metal-rich clusters, and $\sigma = 356 \pm 25$ km s $^{-1}$ for the metal-poor clusters where the uncertainties have been determined from bootstrapping. These are uncorrected for any rotation, but as we show below, the rotation is small and does not affect the dispersions significantly. Moreover, regardless of its origin, the difference in velocity dispersions provides dynamical evidence for the original distinction between the metal-rich and metal-poor cluster populations in NGC 4472.

It is also interesting to note that the difference in dispersions between the metal-rich and metal-poor globular cluster populations in NGC 4472 does not necessarily imply that the populations have different orbital properties. This is because there is observational evidence that the metal-rich cluster system in NGC 4472 is more spatially concentrated than the metal-poor cluster system (e.g. Lee et al. 1998). This difference between the density profiles of the metal-poor and metal-rich globular cluster populations makes it possible for these populations to have similar orbital anisotropy but different velocity dispersions, and still follow the same gravitational potential. In detail, the velocity dispersion difference we observe is modestly larger ($\sim 2\sigma$) than that expected from the difference in the spatial distributions for the metal-poor and metal-rich clusters found by Lee et al. (1998).

3.2. Rotation

A second major goal of our spectroscopic study of the NGC 4472 globular cluster system was to determine the rotation of the system as a whole, as well as that of the metal-rich and metal-poor populations. As discussed in the introduction, determining the rotation of the cluster populations in NGC 4472 is invaluable for addressing questions about the formation history of the galaxy and the relationship of the different cluster populations to one another.

A straightforward way to estimate the rotation in the globular cluster system of NGC 4472 is to do a non-linear least-squares fit to the equation

$$V(r) = V_{rot} \sin(\theta - \theta_0) + V_o. \quad (1)$$

This determines the best fitting flat-rotation curve with the position angle of the line of nodes (θ_0) and the rotation velocity (V_{rot}) free parameters. The results from this analysis are given in Table 3. We find little or no rotation in the metal-rich population and modest evidence for rotation in the full sample and in the metal-poor population. The line of nodes of the best fitting rotation solution appears to be similar to the position angle of the major axis of the galaxy ($PA \simeq 172^\circ$). The significance of the rotation detections can be tested by performing Monte Carlo simulations of the data. These simulations retain the position angles of the objects but randomize the velocities (cf. S98). Roughly half of such simulations give a rotation signature about some axis equal to that observed in the metal-poor and total cluster samples. However, the rotation in these simulations is not preferentially aligned with the major axis of the galaxy, as the real data is. We can account for this by considering random samples with the position angle of the line of nodes fixed to be that observed for the isophotes the galaxy. In this case, only 16% of the random simulations

give a rotation signature as large as observed for the total and metal-poor cluster samples. The metal-rich sample still does not show evidence for rotation even when the position angle is fixed.

In addition to the best fitting rotation solution, we determine an upper limit on the rotation by creating Monte Carlo samples of clusters with the same number of objects and the same velocity dispersion as the given populations, but with a given rotation velocity. We define the 99% confidence upper limit as the rotation velocity for which only 1/100 of such random samples gives a rotation signature as small as that observed. This procedure produces strict upper limits on the rotation in the globular cluster system of NGC 4472, especially the metal-rich population. Specifically, the 99% upper limit on rotation for the full cluster sample is 120 km s^{-1} , for the metal-poor cluster population the 99% upper limit on rotation is 200 km s^{-1} , and for the metal-rich population the rotation is less than 75 km s^{-1} at 99% confidence.

These limits on rotation can be used to set upper limits on the ratio of $(v/\sigma)_{proj}$, which is a common diagnostic of the importance of rotation. For the metal-rich population, the combination of the 99% upper limit of 75 km s^{-1} on the rotation with the velocity dispersion of 221 km s^{-1} found earlier gives an upper limit of $(v/\sigma)_{proj} < 0.34$ at 99% confidence. This is remarkably low compared to the expectation of simple collapse models. It is also dramatically lower than the metal-rich thick disk/bulge clusters of the Milky Way, which have $v/\sigma > 1$. Although the value for NGC 4472 is a projected one, it is very unlikely that rotation is dynamically significant. One way to see this is to compare the observed $(v/\sigma)_{proj}$ of the metal-rich cluster system in NGC 4472 to that expected for an oblate rotator (e.g. Binney & Tremaine 1987). For the observed ellipticity of about 0.2 for the metal-rich population (Lee et al. 1998, Rhode & Zepf 2000), an oblate rotator would have a $(v/\sigma)_{proj}$ of about 0.4, mostly independent of projection. This prediction for an oblate rotator is larger than the 99% upper limit, strongly suggesting that the metal-rich globular cluster system of NGC 4472 is not supported by rotation. A similar approach is to note that the inclination would have to be $i < 12^\circ$ for $(v/\sigma)_{proj} = 0.34$ to be consistent with $v/\sigma \geq 1$. Moreover, such an inclination would require an intrinsic flattening of greater than E9 for the metal-rich system to match the observed E2 in projection.

The very small rotation in the metal-rich globular cluster system of NGC 4472 is problematic for models in which central spheroidal systems all form similarly, with the only difference being the mass of the central bulge/elliptical component. Instead, it requires efficient angular momentum transport for the metal-rich globular cluster population of NGC 4472 that did not occur during the formation of the metal-rich globular cluster population of the Milky Way. Such a difference is natural in models in which elliptical galaxies like NGC 4472 formed in major mergers, and spiral galaxies formed in such a way as to avoid disruptive events that lead to effective, large scale transport of angular momentum. This is discussed in more detail in the final section of the paper.

3.3. Radial Variations of Rotation and Velocity Dispersion

In addition to the total velocity dispersions and rotation velocities derived in the two previous sections, radial trends in these quantities are also interesting. For example, if the velocity dispersion can be traced out to large radii, constraints can be placed on the mass distribution of the halo, although some simplifying assumptions about the orbital anisotropy of the globular cluster population are required for modest sample sizes. Conversely, a mass distribution can be adopted based on other data such as X-ray observations, and then the observed dispersions can be used to constrain the orbital anisotropy at different radii. Similarly, changes in the rotation velocity as a function of radius can be used to trace the distribution of angular momentum within a galaxy.

In order to determine the rotational velocity and velocity dispersion as a function of radius, it is necessary to average in some way the discrete radial velocities of individual clusters. Binning is not ideal because of its well-known sensitivity to the choice of bin centers and sizes. The problem of estimating smooth functions from individual datapoints is a well-developed statistical field (e.g. Simonoff 1996 and references therein). The application of these techniques to the problem of estimating the velocities and dispersion of the globular cluster systems as a function of radius is straightforward because our goal is to determine the overall trends in these systems and sharp changes are not expected. In this case, a Gaussian smoothing kernel provides reliable results with the advantage of simplicity in application and interpretation.

A key question for any smoothing procedure is to determine the width of the smoothing kernel. A common approach, called cross-validation, is to determine the kernel size that minimizes the summed total of the variances determined at each point, when that point is excluded from the calculation. However, cross-validation gives little guidance when the sample in question is consistent with being a constant, because it is statistically preferable in this case to use all of the data to determine the value of the function in question at each radius. This is exactly the case for the velocities of the globular cluster system of NGC 4472, particularly the full sample and the metal-poor subsample. Therefore, while cross-validation clearly identifies the statistical consistency of the data with a flat rotation curve, it does not yield much help for determining the appropriate smoothing kernel for determining any dependence of the velocity dispersion on radius. Because our goal is to determine the overall trend of velocity dispersion with radius, we adopt a fairly broad smoothing, using a Gaussian kernel with $\sigma = 100''$. This kernel width is roughly equivalent to two or three independent radial “bins.” Smaller smoothing kernels produce the same overall trends, with additional bumps and wiggles. A sign that these may be undersmoothed is that the velocity dispersion profiles from smaller kernels yield unphysical results when used in the Jeans equation (see Section 3.4).

Figure 3 shows the results of our analysis of the radial variation of the rotation and velocity dispersion. Because the line of nodes of rotation is consistent with the position angle of the galaxy (Section 3.2), the data have been flipped about the minor axis to take full advantage

of the available positions and velocities. The upper and lower lines are 1σ bootstrap limits. In order to build the bootstrap samples in a way that is consistent with the smoothing kernel used to determine the best fit, the probability of including an object in the bootstrap sample is proportional to the value of the kernel of that object at a given radius. Because of the smoothing required to get rotation and velocity dispersions from individual radial velocities, the individual points along the curves are of course not independent of one another.

Overall, the globular cluster population in NGC 4472 appears to have a slowly declining velocity dispersion with radius. This is seen in the full sample, and the individual metal-rich and metal-poor samples are consistent with the same trend. A sharper drop in the dispersion at our largest radial distances ($r \gtrsim 400''$) is also consistent with the data, as shown by the lower limit of the dispersion in Figure 3 and also by analyses using smaller smoothing kernels. Further data at large radii is required to test this possibility. The slightly declining velocity dispersion in NGC 4472 contrasts to the slightly rising dispersion found for M87 over the same radial range (e.g. Cohen 2000 and references therein). This difference may suggest that the rising dispersion in M87 is due to transition from the galaxy to the Virgo cluster itself, as M87 is located at the center of the Virgo cluster, while NGC 4472 is well away from the cluster center.

Figure 3 also shows the rotational velocity of the total sample and the metal-poor population is consistent with a constant value at all radii, while the metal-rich sample shows slight evidence for increasing rotation outwards. This can also be seen by performing a straight regression of velocity with major axis distance, which gives absolutely no trend for the total and metal-poor samples, and a 1σ result for increasing rotation with larger radii for the metal-rich sample. At all radii for which we have data the rotation is significantly smaller than the dispersion. This applies to the globular cluster sample as a whole, as well as to the metal-rich and metal-poor cluster populations.

3.4. M/L ratio and Orbital Isotropy

The velocity dispersion profile determined in the previous section can be used to derive the mass distribution of NGC 4472 through the application of the Jeans equation (e.g. Binney & Tremaine 1987). The mass determined in this way depends on the anisotropy of the cluster orbits, as well as on the directly observed projected velocity dispersion and projected density profiles. The simplest approach is to adopt isotropy for the cluster orbits, and to see how this compares to other estimates for the mass of NGC 4472 within the same radial range. In detail, the three dimensional luminosity density and velocity dispersion profiles are determined from the observed projected quantities by numerically integrating the Abel equations. Spherical symmetry is assumed in this approach, which is not strictly true for NGC 4472, but it is not likely to be too far wrong given that the observed ellipticity of the globular cluster systems is 0.1 – 0.2 (e.g. Lee et al. 1998).

Figure 4 shows the mass of NGC 4472 as a function of radius. The lines are masses inferred

from application of the Jeans equation to the radial velocities of our globular cluster sample. The central solid line is the best fit to the 144 radial velocities discussed in this paper. The dotted lines are the 1σ lower and upper limits. These uncertainties in the mass are based on the bootstrapped uncertainties in the radial velocity dispersion profile given in the previous section. We do not include uncertainties in the density profile of the globular cluster system because they are much smaller than those for the velocity dispersion. Specifically, the surface density profile is taken from the fit of a de Vaucouleurs' law to the wide field CCD imaging study of Rhode & Zepf (2000), which extends out to $\gtrsim 20'$, well beyond our last data point. Different techniques for deriving the density profile from these data or comparisons to previous work produce variations that are much smaller than the uncertainty in the velocity dispersion.

The radial profile of the mass distribution of NGC 4472 derived from the radial velocities of the globular clusters can be compared to the mass inferred from X-ray observations of the hot gas around the galaxy. The solid squares on Figure 4 are the masses inferred from ROSAT observations of the hot gas around NGC 4472 (Irwin & Sarazin 1996). The open squares represent points for which the assumption of hydrostatic equilibrium on which the X-ray masses are based may be uncertain because the X-ray isophotes are irregular at these radii.

The overall agreement between the mass inferred from the globular cluster velocities given isotropic orbits and the mass inferred from the analysis of X-ray observations of the hot gas assuming hydrostatic equilibrium is good. This agreement suggests that both assumptions are probably roughly correct, and that the masses so derived are reasonably accurate. The conclusion that then follows is that the mass-to-light ratio of NGC 4472 is at least five times greater at radii of ~ 30 kpc than it is at radii of several kpc, indicative of a substantial dark halo around this galaxy. This is some of the strongest dynamical evidence to date for massive halos around elliptical galaxies. At small radii, there is a hint that the mass inferred from the globular cluster dynamics may be slightly higher than that inferred from the hot gas. This could either be the result of statistical uncertainties in either observation, a slight radial anisotropy in the globular cluster orbits at smaller radii, or a slight underestimation of the temperatures in the hot gas at small radii. In any case the overall agreement between the two approaches is good, and more data will be required to extend this approach to larger radii and to test for any differences at smaller radii.

4. Implications

One of the primary goals of the study of the kinematics of the globular cluster systems of nearby ellipticals is to constrain the formation history of these galaxies. The bimodal color distributions of the globular cluster systems of many ellipticals already indicate an episodic formation history for these galaxies, roughly along the lines predicted by merger models. The kinematic data presented here confirm and extend the identification of two populations of globular clusters in NGC 4472 by showing that the population of globular clusters identified as metal-poor

through their colors has a higher velocity dispersion than the population identified as metal-rich.

In addition to confirming the existence of a metal-rich and metal-poor globular cluster populations in NGC 4472, our data help constrain the physical nature of the episodic formation history of this galaxy. Perhaps the most critical observational result is that there is little or no rotation in the metal-rich globular cluster system. Despite the absence of rotation, the metal-rich system clearly underwent significant dissipation and collapse since it is more spatially concentrated than the metal-poor cluster population and much more so than the dark matter halo. Given conservation of angular momentum, the metal-rich population would be naturally expected to spin up as it collapses. In fact, significant rotation is observed in the metal-rich population of disk galaxies like the Milky Way and M31. Thus the minimal rotation in the metal-rich globular cluster population of NGC 4472 requires angular momentum transport during the formation of this elliptical galaxy, and distinguishes the metal-rich globular cluster population in this elliptical from metal-rich cluster populations in the Galaxy and M31. Merger models have long been put forward as a way to transport angular momentum outwards (e.g. Toomre & Toomre 1972, Barnes & Hernquist 1992 and references therein). A generally consistent picture can be constructed in which elliptical galaxies like NGC 4472 form in major mergers which create the metal-rich globular cluster population and transfer angular momentum outwards, while disk galaxies like the Milky Way and M31 have only had more minor mergers, which may lead to modest amounts of globular cluster formation but which are not as efficient at angular momentum transfer.

An additional implication of our data is that NGC 4472 has a dark halo that extends out to the limit of our dataset, about 30 kpc. However, this limit is only set by the field of view of the spectrographs we have used. A wide-field CCD imaging study of the globular cluster system of NGC 4472 shows that it extends out to at least 80 kpc (Rhode & Zepf 2000). Thus globular clusters offer a dynamical probe of the halo at very large radii which can be reached effectively with spectrographs with sufficient field of view. This is particularly valuable for NGC 4472, since its X-ray isophotes are irregular at radii greater than about 20 kpc, indicating the hot gas may not be in hydrostatic equilibrium. Without hydrostatic equilibrium, mass estimates from X-ray gas are problematic, leaving dynamical techniques the best hope for extending the understanding of the halo of NGC 4472 to very large radii.

5. Conclusions

In this paper, we present radial velocities for 144 globular clusters around NGC 4472. Based on this dataset, we analyze the kinematics of the globular cluster system as a function radius and metallicity. We find

1. The metal-poor globular clusters have a significantly higher velocity dispersion than the metal-rich clusters. This kinematic difference confirms the identification of these two cluster populations within NGC 4472, as they were originally selected based on their colors alone.

2. $(v/\sigma)_{proj}$ is much less than one over the radial range covered by our data ($\sim 3 - 30$ kpc). This is true for the globular cluster system as a whole and for the individual metal-rich and metal-poor cluster systems. The upper limit on rotation is particularly small for the metal-rich globular cluster system, for which $(v/\sigma)_{proj} < 0.34$ at the 99% confidence level.

3. This absence of rotation requires either significant angular momentum transport outwards during the formation of NGC 4472 or a much lower initial spin of the halo of NGC 4472 than given by standard tidal torque calculations. The requirement for significant angular momentum transport is particularly strong for the metal-rich population, which is concentrated towards the center of the galaxy and has a high metallicity. These properties point to significant dissipation and collapse during the formation of the metal-rich cluster population, yet it has little or no rotation.

4. The absence of significant rotation in the metal-rich globular cluster population of NGC 4472 strongly distinguishes this metal-rich cluster population from the metal-rich cluster populations found in disk galaxies like the Milky Way. Thus the angular momentum transport required for the metal-rich cluster population in NGC 4472 appears to be associated with the physical differences between elliptical and spiral galaxies. This may be explained if ellipticals form from major mergers, while spirals are those galaxies that have not had major mergers since the formation of their disk.

5. The velocity dispersion profile of the NGC 4472 slowly declines with radius, with a hint that the decline may steepen at large radius. The mass derived from this dispersion profile and the assumption of isotropic orbits is consistent with that derived from X-ray observations of the hot gas. This suggests that neither technique has dramatic systematic problems, and strongly indicates the presence of a dark matter halo around NGC 4472.

We thank Dave Carter for his contributions to the early stages of the research project, David Buote for making available his analysis of the ROSAT observations of NGC 4472, and the referee for a careful reading of the paper. We acknowledge useful conversations with Ken Freeman, Melinda Weil, and Dean McLaughlin. SEZ acknowledges support from the Hellman Family Foundation, MAB acknowledges the support of a PPARC studentship and the use of STARLINK facilities at the University of Durham, DG acknowledges support for this project from CONICYT through Fondecyt grant 1000319 and by the Universidad de Concepción through research grant No. 99.011.025-1.0, and DAH acknowledges support from an Operating Grant awarded by the Natural Sciences and Engineering Research Council (NSERC) of Canada.

REFERENCES

Ashman, K.M., & Zepf, S.E. 1992, ApJ, 384, 50
Ashman, K.M., & Zepf, S.E. 1998, Globular Cluster Systems, (Cambridge: Cambridge University

Press)

Barger, A.J., Cowie, L. L., Trentham, N., Fulton, E., Hu, E. M., Songaila, A., & Hall, D. 1999, AJ, 117, 102

Barnes, J.E., & Efstathiou, G. 1987, ApJ, 319, 575

Barnes, J.E., & Hernquist, L. 1992, ARA&A, 30, 705

Beasley, M.A., et al. 2000, MNRAS, in press

Benitez, N., Broadhurst, T.J., Bouwens, R., Silk, J., & Rosati, P. 1999, ApJ, 515, L65

Binney, J., & Tremaine, S. 1987, Galactic Dynamics, (Princeton: Princeton University Press)

Cohen, J.C. 2000, AJ, 119, 162

Cohen, J.C., & Ryzhov, A. 1997, ApJ, 486, 230

Coppi, P. S., & Zepf, S.E. 2000, ApJ, in preparation

Cote, P., Marzke, R.O., & West, M.J. 1998, ApJ, 501, 554

Crampton, D. et al. 1992, Proc. ESO Conference on Progress in Telescope and Instrumentation Technologies, ed. M.-H. Ulrich, 609

Eisenstein, D.J., & Loeb, A. 1995, 439, 520

Fall, S.M. 1979, Nature, 281, 200

Fall, S.M., & Efstathiou, G. 1980, MNRAS, 193, 133

Forbes, D.A., Brodie, J.P., & Grillmair, C.J. 1997, AJ, 113, 1652

Fukugita, M., Hogan, C.J., & Peebles, P.J.E. 1998, ApJ, 503, 518

Geisler, D., Lee, M.G., & Kim, E. 1996, AJ, 111, 1529

Gebhardt, K., & Kissler-Patig, M. 1999, AJ, 118, 1526

Harris, W.E., Harris, G.L.H., & McLaughlin, D.E. 1998, AJ, 115, 1801

Heavens, A., & Peacock, J. 1988, MNRAS, 232, 339

Irwin, J.A., & Sarazin, C.L. 1996, ApJ, 471, 683

Kauffmann, G., & Charlot, S. 1998, MNRAS, 294, 705

Kissler-Patig, M., & Gebhardt, K. 1998, AJ, 116, 2237

Kodama, T., & Arimoto, N. 1997, A&A, 320 41

Kundu, A. 1999, PhD. Thesis, University of Maryland

Lee, M.G., Kim, E., & Geisler, D. 1998, AJ, 115, 947

Lee, M.G., & Kim, E. 2000, AJ, in press (astro-ph/0004116)

Le Fevre, O., Crampton, D., Felenbok, P., & Monnet, G. 1994, A&A, 282, 325

McLaughlin, D.E. 1999, AJ, 117, 2398

Merritt, D., & Tremblay, B. 1994, AJ, 108, 514

Mould, J.R., Oke, J.B., de Zeeuw, P.T., & Nemec, J.M. 1990, AJ, 99, 1823

Puzia, T.H., Kissler-Patig, M., Brodie, J.P., & Huchra, J.P. 1999, AJ, 118, 2734

Rhode, K.L., & Zepf, S.E., 2000, AJ, submitted

Schweizer, F. 1998, in Galaxies: Interactions and Induced Star Formation, Saas-Fee Course 26, eds. R.C. Kennicutt et al. (Springer: Berlin), 105

Sharples, R.M., Zepf, S.E., Bridges, T.J., Hanes, D.A., Carter, D., Ashman, K.M, & Geisler, D. 1998, AJ, 115, 2337

Silk, J., & Wyse, R.F.G. 1993, Physics Reports, 231, 293

Siminoff, J.S. 1996 Smoothing Methods in Statistics (Springer: New York)

Tonry, J., & Davis, M. 1979, AJ, 84, 151

Toomre, A., & Toomre, J. 1972, ApJ, 178, 623

Toomre, A. 1977, in The Evolution of Galaxies and Stellar Populations, eds. B. Tinsley & R. Larson (Yale Univ. Press), 401

Treu, T., et al. 1998, A&A, 340, L10

Treu, T., & Stiavelli, M. 1999, ApJ, 524, L27

Warren M. S., Quinn, P. J., Salmon, J. K., & Zurek, W. H. 1992, ApJ, 339, 405

Woodworth, S.C., & Harris, W.E.H 2000, AJ, 119, 2699

Zepf, S.E., & Ashman, K.M. 1993, MNRAS, 264, 611

Zepf, S.E., Ashman, K.M., & Geisler, D. 1995, ApJ, 443, 570

Zepf, S.E. 1997, Nature, 390, 377

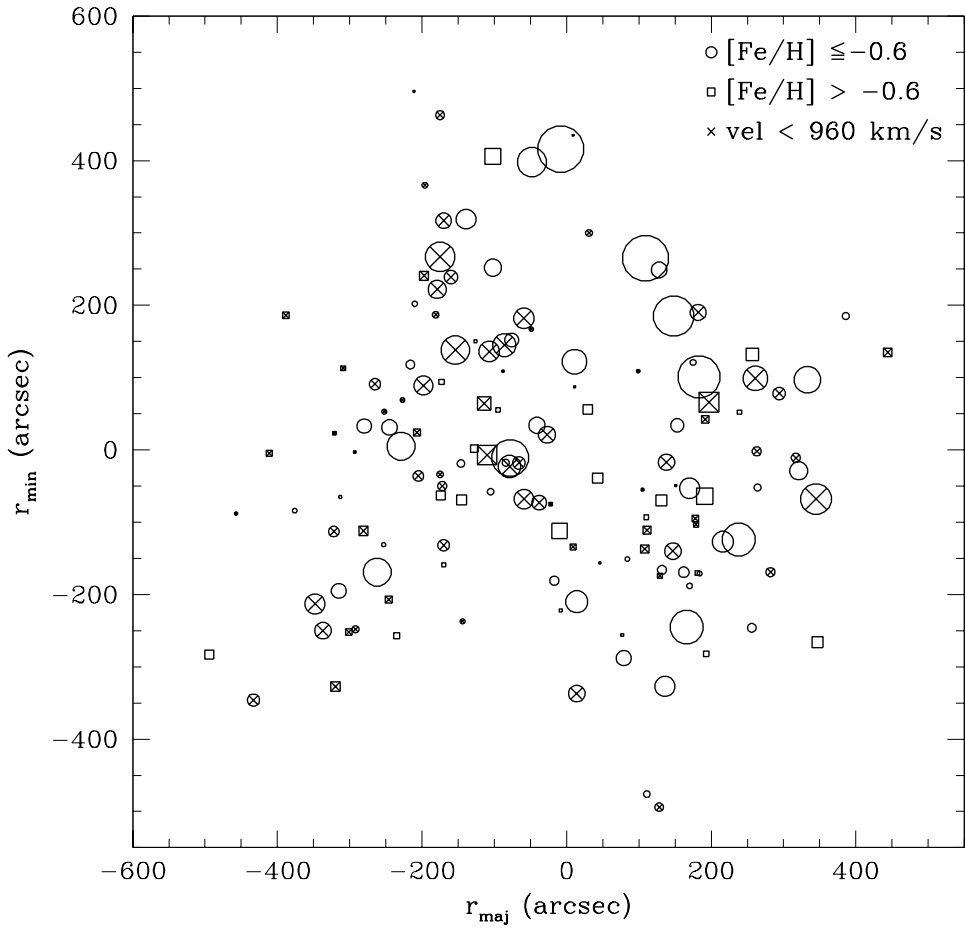


Fig. 1.— A plot of the location and velocities for our NGC 4472 globular cluster dataset. The clusters are plotted at their location on the sky, with a symbol size proportional to their velocity difference from the systemic velocity of NGC 4472. An x indicates a negative velocity with respect to the velocity of the galaxy, and an open symbol indicates a positive velocity. Globular clusters identified by their colors as part of the metal-rich population are plotted as squares, and globular clusters in the metal-poor population are plotted as circles. This plot shows that the dispersion falls off gradually with radius, and that there is no obvious rotation about any axis, especially for the metal-rich cluster population.

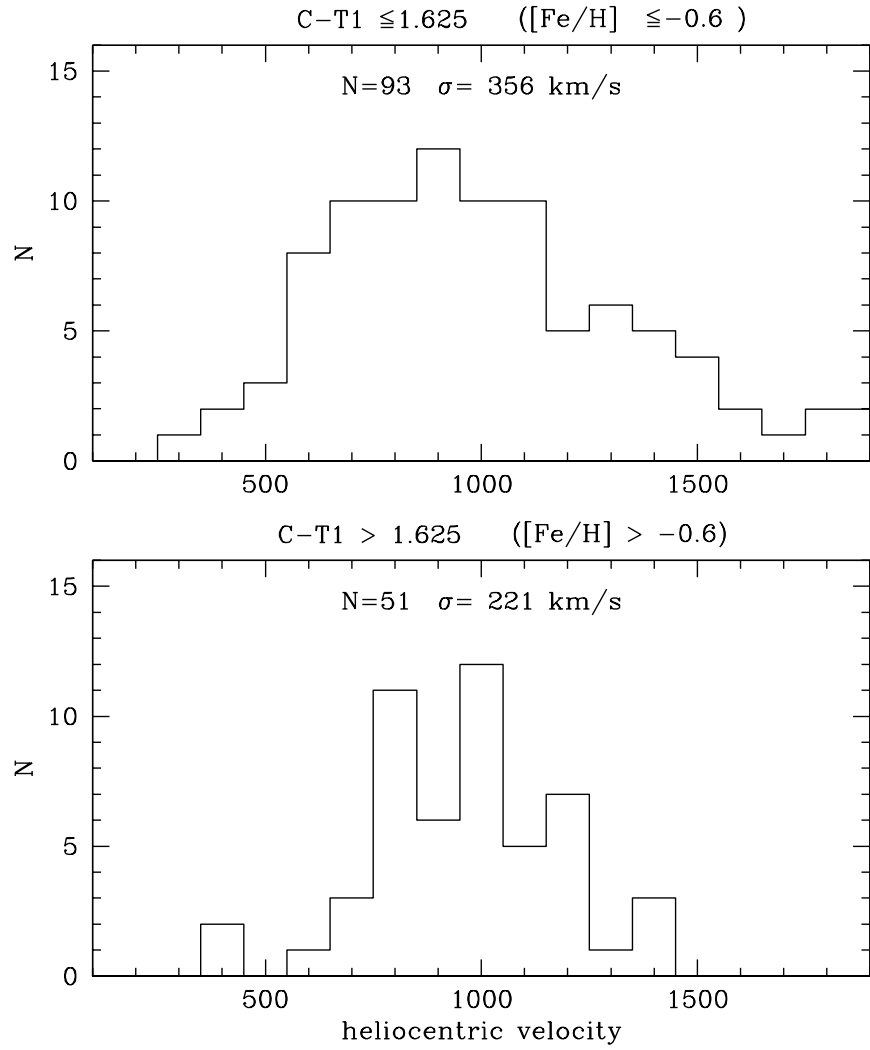


Fig. 2.— Histograms of the velocities for the metal-poor (upper panel) and metal-rich (lower panel) globular cluster populations in NGC 4472. The larger velocity dispersion of the metal-poor clusters is clearly evident. A F-test indicates that this difference is significant at greater than 99%. This provides independent confirmation of the original identification of metal-rich and metal-poor populations of globular clusters in this galaxy.

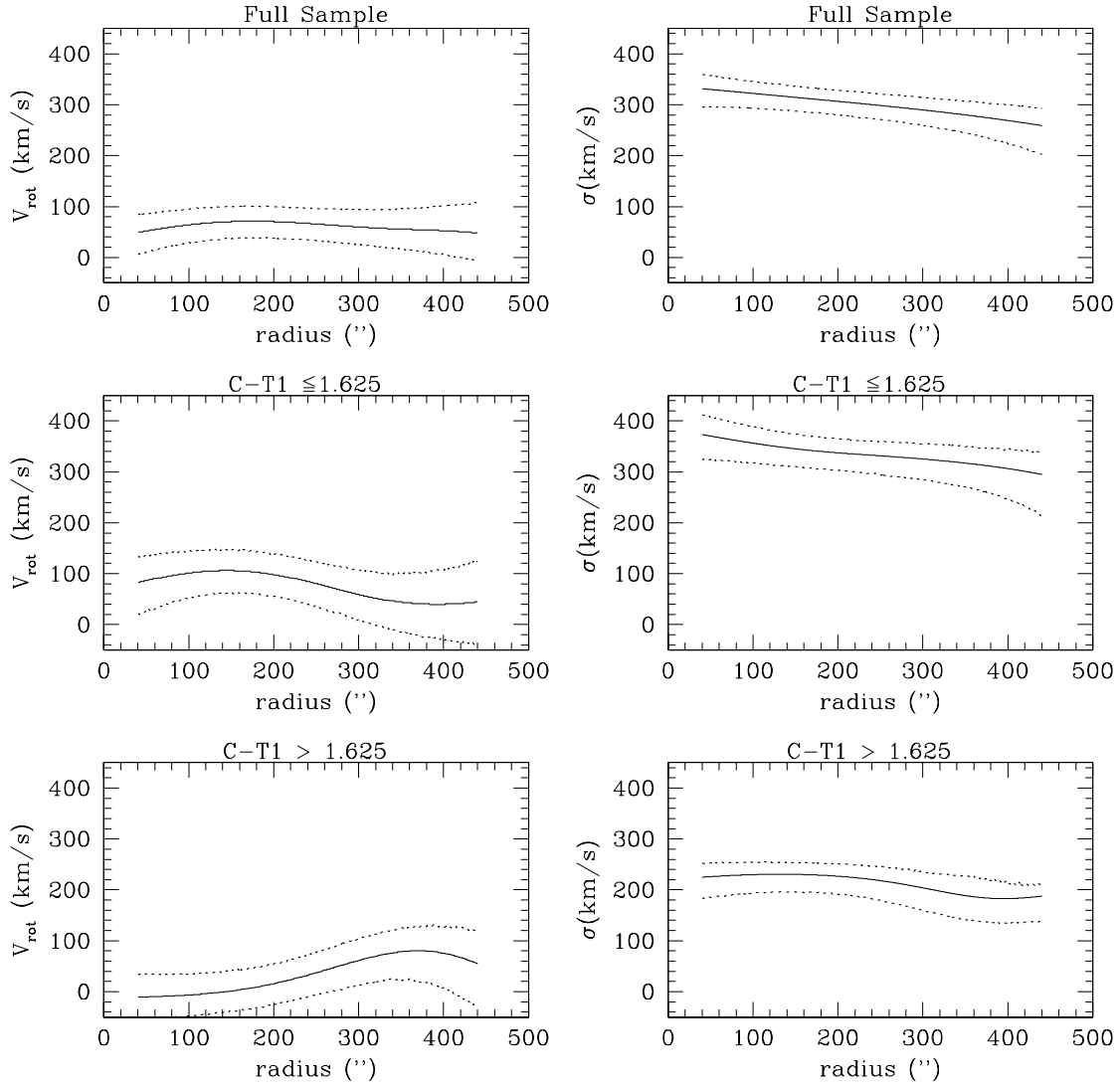


Fig. 3.— Plots of the rotation and velocity dispersion fields for the globular clusters of NGC 4472. The top panels are for the full data set, the middle panels for the metal-poor (blue) clusters and the bottom panels for the metal-rich (red) clusters. A Gaussian kernel with $\sigma = 100''$ was used for the radial smoothing for all of the datasets. The dotted lines show the 1σ uncertainties, as determined from bootstrapping. The curves are highly correlated in the radial direction with the smoothing used. The plots show modest rotation in the full sample and the metal-poor cluster population which is essentially constant with radius. The red sample has essentially zero rotation at small radius and a tentative (1σ) rise to modest rotation at larger radii. The velocity dispersion is significantly larger than the rotation at all radii.

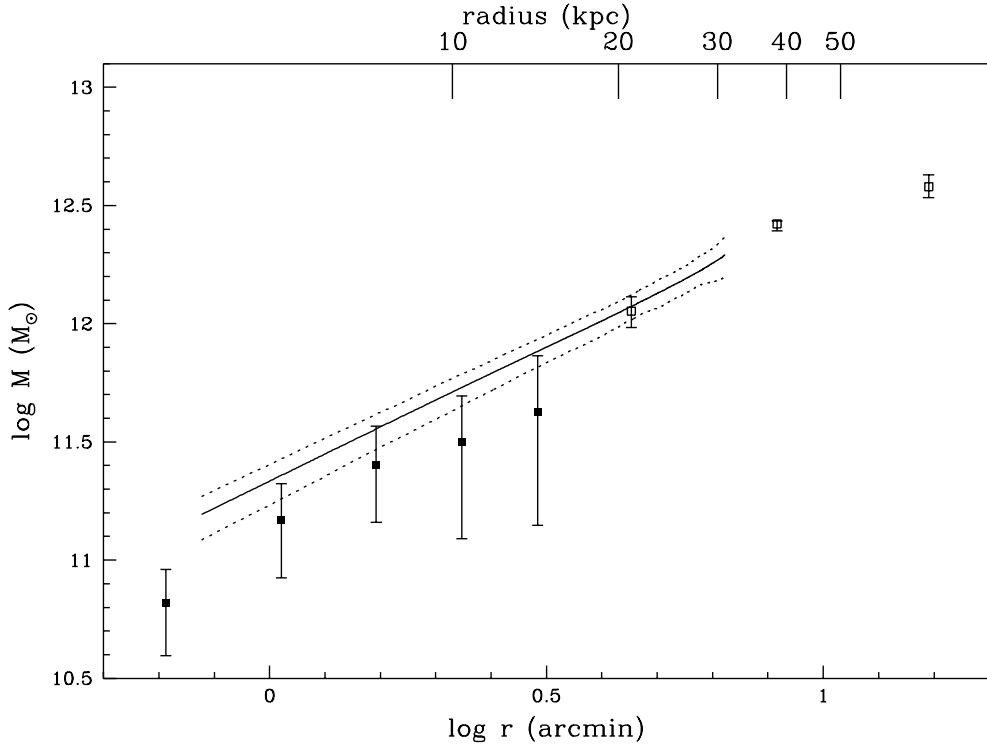


Fig. 4.— A plot of the mass of NGC 4472 as a function of radius. The lines are masses inferred from the radial velocities of the globular clusters. The central solid line is the best fit to the 144 radial velocities discussed in this paper. The dotted lines are the 1σ lower and upper limits determined via bootstrapping. All of these are based on the assumption of isotropic orbits for the globular clusters. The points are masses inferred from ROSAT observations of the hot gas around NGC 4472 (Irwin & Sarazin 1996). The open squares represent points for which the assumption of hydrostatic equilibrium on which the X-ray masses are based may be uncertain because the X-ray isophotes are irregular at these radii. The overall agreement between the masses inferred from the two techniques is good, suggesting that the assumptions underlying each approach are probably roughly correct. The conclusion that then follows is that NGC 4472 has a substantial dark halo, with a mass-to-light ratio at several tens of kpc that is at least a factor of five greater than in the inner regions of the galaxy.

Table 1. Velocities of Globular Clusters in NGC 4472

ID ¹	R.A. (B1950.0)	Decl. (B1950.0)	T ₁ (mag)	C-T ₁ (mag)	V _{hel} (km s ⁻¹)
170	12 27 05.19	8 09 52.6	21.19	1.73	1243 ±69
282	12 27 32.88	8 10 24.1	20.38	1.65	751 ±39
463	12 27 17.87	8 10 55.5	19.93	1.59	342 ±27
637	12 27 10.03	8 11 24.1	19.95	1.54	814 ±31
647	12 27 04.56	8 11 25.4	21.15	1.34	1101 ±39
676	12 27 19.80	8 11 30.5	20.72	1.46	1304 ±56
714	12 27 34.88	8 11 35.4	20.32	1.55	1061 ±39
744	12 27 20.91	8 11 40.2	19.73	1.38	814 ±29
876	12 27 28.14	8 11 58.3	19.63	1.46	1487 ±24
995	12 26 46.05	8 12 10.0	20.90	1.54	828 ±90
1047	12 27 00.94	8 12 13.8	21.14	1.89	1083 ±30
1087	12 27 17.20	8 12 17.5	19.64	1.44	1070 ±29
1110	12 27 12.04	8 12 20.3	19.88	1.37	1626 ±24
1207	12 27 26.09	8 12 29.3	21.34	1.25	739 ±69
1234	12 26 46.82	8 12 32.2	20.81	1.47	1059 ±64
1255	12 27 20.37	8 12 34.4	19.71	1.35	816 ±66
1315	12 27 11.39	8 12 40.9	20.68	1.42	1370 ±76
1423	12 27 02.74	8 12 51.3	20.94	1.57	1641 ±29
1448	12 26 56.90	8 12 54.2	20.79	1.34	1353 ±26
1475	12 27 07.89	8 12 57.0	21.15	1.46	1018 ±37
1518	12 27 07.89	8 13 00.6	19.25	1.85	1050 ±36
1570	12 27 06.52	8 13 05.6	20.98	1.58	1034 ±61
1587	12 27 26.80	8 13 07.3	21.16	1.12	471 ±75
1650	12 27 23.30	8 13 13.6	20.85	1.95	1040 ±55
1712	12 27 07.54	8 13 19.0	20.36	1.34	1144 ±40
1731	12 27 28.81	8 13 21.1	20.71	1.82	1294 ±51
1749	12 27 14.86	8 13 22.6	20.92	1.98	1407 ±88
1764	12 27 12.15	8 13 23.6	20.82	1.72	855 ±37
1798	12 27 12.65	8 13 25.9	20.69	1.98	811 ±31
1982	12 27 9.12	8 13 42.0	20.89	1.01	648 ±43
2031	12 27 15.13	8 13 46.4	20.71	1.37	1352 ±65
2045	12 27 6.50	8 13 47.8	20.94	1.77	857 ±54
2060	12 27 7.15	8 13 48.3	20.62	1.29	1108 ±65
2140	12 27 21.65	8 13 55.5	20.45	1.80	784 ±31
2163	12 27 23.34	8 13 57.7	20.15	2.01	402 ±43
2195	12 26 58.16	8 14 00.8	21.33	1.14	1241 ±56

Table 1—Continued

ID ¹	R.A. (B1950.0)	Decl. (B1950.0)	T ₁ (mag)	C-T ₁ (mag)	V _{hel} (km s ⁻¹)
2256	12 27 14.99	8 14 05.8	21.24	1.90	954 ±28
2341	12 27 00.22	8 14 13.0	20.76	1.91	1001 ±68
2406	12 27 13.24	8 14 18.5	20.84	2.03	1244 ±70
2420	12 27 08.45	8 14 19.3	20.95	2.08	763 ±92
2452	12 27 25.28	8 14 22.5	21.49	1.40	1828 ±81
2482	12 27 10.16	8 14 24.7	21.58	2.08	767 ±56
2528	12 27 16.79	8 14 28.3	20.34	1.46	654 ±65
2543	12 27 20.34	8 14 29.3	20.27	1.36	1199 ±48
2569	12 27 11.33	8 14 31.7	20.12	1.89	1056 ±46
2634	12 27 07.09	8 14 38.0	19.70	1.56	1014 ±57
2753	12 27 13.65	8 14 47.0	20.88	1.19	945 ±100
2759	12 26 53.73	8 14 47.3	19.97	1.31	654 ±92
2817	12 27 30.93	8 14 50.6	21.05	1.50	665 ±47
3150	12 27 05.95	8 15 12.2	21.40	1.79	952 ±42
3307	12 27 29.92	8 15 21.4	20.25	1.53	1790 ±65
3361	12 27 01.91	8 15 26.6	20.34	1.55	1392 ±33
3628	12 27 00.59	8 15 44.0	21.22	1.90	1008 ±49
3635	12 27 24.04	8 15 44.5	20.86	1.34	936 ±94
3757	12 27 13.40	8 15 51.8	21.02	1.82	1220 ±95
3808	12 27 06.60	8 15 54.6	20.35	1.83	832 ±35
3909	12 27 33.58	8 16 00.4	21.43	1.36	1253 ±90
3980	12 27 03.05	8 16 05.4	21.15	1.28	1112 ±45
4168	12 27 07.64	8 16 19.4	20.36	1.68	1384 ±44
4210	12 27 34.25	8 16 22.9	20.53	1.62	1910 ±29
4386	12 27 19.17	8 16 34.7	19.83	1.94	1197 ±33
4513	12 27 09.78	8 16 42.8	20.10	1.85	908 ±80
4731	12 27 09.56	8 16 58.2	19.96	1.43	698 ±57
4780	12 27 20.80	8 17 00.9	19.52	1.95	971 ±45
4959	12 27 23.06	8 17 11.9	21.38	1.33	1449 ±44
5090	12 27 09.43	8 17 20.3	19.83	1.61	582 ±46
5323	12 27 16.29	8 17 33.9	20.33	0.82	1263 ±65
5456	12 27 12.49	8 17 41.4	19.26	1.39	737 ±65
5561	12 26 56.85	8 17 48.3	20.82	1.39	903 ±48
5564	12 27 34.86	8 17 48.5	21.26	1.37	862 ±19
5629	12 27 11.90	8 17 52.3	21.09	1.36	522 ±52
5707	12 27 12.63	8 17 55.9	21.47	1.44	1712 ±30

Table 1—Continued

ID ¹	R.A. (B1950.0)	Decl. (B1950.0)	T ₁ (mag)	C–T ₁ (mag)	V _{hel} (km s ^{–1})
5750	12 27 12.08	8 17 58.9	21.50	1.47	1063 ±89
5856	12 27 09.09	8 18 06.4	21.03	1.13	1050 ±84
6108	12 27 24.66	8 18 22.8	21.49	1.42	913 ±39
6164	12 27 12.26	8 18 27.2	19.79	1.65	426 ±30
6231	12 27 16.55	8 18 32.3	20.77	1.82	1046 ±50
6284	12 27 25.39	8 18 36.8	19.44	1.57	569 ±54
6294	12 27 01.30	8 18 37.7	21.02	1.64	1034 ±84
6344	12 27 07.59	8 18 41.3	20.89	2.01	1220 ±50
6357	12 27 20.14	8 18 41.9	20.47	1.26	958 ±29
6388	12 27 23.15	8 18 44.5	20.18	1.36	1212 ±24
6394	12 27 03.03	8 18 45.0	21.40	1.42	760 ±85
6427	12 27 12.47	8 18 47.5	21.11	1.79	1141 ±50
6476	12 27 43.03	8 18 50.2	20.94	2.23	966 ±36
6485	12 27 22.50	8 18 51.2	21.07	1.53	510 ±82
6520	12 27 16.76	8 18 53.6	20.06	1.86	607 ±57
6564	12 27 10.77	8 18 57.3	20.03	1.34	1077 ±31
6615	12 27 41.49	8 19 01.3	20.48	1.47	1923 ±49
6696	12 27 21.46	8 19 08.5	20.08	1.59	561 ±23
6701	12 26 53.65	8 19 08.6	20.97	2.00	1092 ±141
6721	12 27 07.36	8 19 10.5	21.09	1.73	1180 ±45
6748	12 27 08.24	8 19 12.4	20.21	1.53	817 ±20
6872	12 27 09.21	8 19 20.8	20.15	1.46	870 ±41
6989	12 27 22.00	8 19 30.6	20.61	1.75	1009 ±24
7028	12 27 39.52	8 19 33.5	21.40	1.38	1548 ±39
7043	12 26 56.69	8 19 34.4	20.47	1.78	808 ±67
7095	12 27 29.05	8 19 39.8	21.43	1.56	1285 ±80
7197	12 27 08.44	8 19 48.2	20.94	1.50	782 ±50
7281	12 27 20.64	8 19 53.8	21.43	1.25	389 ±123
7340	12 27 17.40	8 19 59.0	20.91	1.77	1067 ±29
7364	12 26 58.73	8 20 01.4	21.36	1.36	1522 ±100
7399	12 27 01.33	8 20 05.1	20.35	1.40	1005 ±44
7430	12 26 53.05	8 20 06.5	20.76	1.41	862 ±66
7449	12 26 47.44	8 20 07.7	20.75	1.65	724 ±65
7458	12 27 12.24	8 20 08.7	20.75	1.84	807 ±57
7531	12 26 52.55	8 20 13.5	19.71	2.07	818 ±72
7616	12 27 16.55	8 20 20.2	21.35	1.49	600 ±90

Table 1—Continued

ID ¹	R.A. (B1950.0)	Decl. (B1950.0)	T ₁ (mag)	C–T ₁ (mag)	V _{hel} (km s ^{–1})
7659	12 27 10.56	8 20 24.0	19.87	1.34	1520 ±44
7702	12 27 38.87	8 20 27.4	21.19	1.88	1388 ±58
7746	12 27 27.01	8 20 31.5	21.29	1.42	712 ±68
7784	12 27 23.23	8 20 34.4	19.20	1.52	868 ±51
7798	12 27 32.56	8 20 35.4	20.96	1.39	1340 ±39
7872	12 27 14.71	8 20 42.0	20.33	1.45	908 ±77
7886	12 26 55.98	8 20 43.8	20.62	1.58	1236 ±33
7889	12 27 25.49	8 20 43.5	18.85	1.58	614 ±65
7894	12 27 01.99	8 20 37.3	21.61	1.73	730 ±81
7914	12 27 18.07	8 20 46.4	21.20	1.33	1101 ±29
7938	12 27 11.91	8 20 47.7	20.92	1.44	1251 ±50
7945	12 26 51.93	8 20 48.2	19.79	1.59	651 ±33
8000	12 27 28.43	8 20 53.3	21.08	1.49	368 ±40
8090	12 27 13.14	8 21 00.9	20.51	1.46	903 ±66
8143	12 27 31.74	8 21 04.7	20.96	1.52	672 ±109
8164	12 27 26.33	8 21 06.9	21.32	2.04	738 ±40
8165	12 27 23.58	8 21 06.9	20.22	1.39	1027 ±47
8210	12 26 54.15	8 21 10.1	20.43	1.32	576 ±88
8273	12 27 01.10	8 21 15.9	20.60	1.43	784 ±90
8332	12 27 11.29	8 21 21.1	21.09	1.40	1226 ±100
8353	12 27 08.71	8 21 22.8	20.03	1.98	928 ±40
8357	12 27 04.34	8 21 22.9	20.26	1.45	981 ±61
8384	12 27 15.30	8 21 24.4	21.39	1.41	768 ±54
8596	12 27 34.37	8 21 44.6	19.73	1.31	888 ±31
8653	12 26 43.83	8 21 49.5	20.50	1.26	744 ±44
8712	12 27 40.99	8 21 54.7	20.93	1.49	817 ±63
8740	12 27 09.77	8 21 57.5	21.27	2.14	913 ±106
8890	12 27 15.78	8 22 14.1	20.41	1.88	870 ±65
8919	12 27 01.83	8 22 16.0	19.87	1.45	1014 ±65
9145	12 27 42.37	8 22 39.1	19.79	1.76	973 ±38
9360	12 26 46.61	8 23 06.8	21.00	1.67	1191 ±99
9414	12 27 06.09	8 23 14.3	20.82	1.74	832 ±40
9527	12 26 59.87	8 23 32.0	20.91	1.58	941 ±61
9666	12 27 18.87	8 23 51.3	20.04	1.74	811 ±71
9991	12 27 26.39	8 14 35.5	19.41	1.27	1040 ±65
9992	12 27 15.80	8 17 16.7	19.99	1.48	641 ±65

Table 1—Continued

ID ¹	R.A. (B1950.0)	Decl. (B1950.0)	T ₁ (mag)	C–T ₁ (mag)	V _{hel} (km s ^{–1})

¹ID from Geisler et al. (1996).

Table 2. Foreground Stars and Background Galaxies near NGC 4472 Identified in MOS Spectra

ID ¹	R.A. (B1950.0)	Decl. (B1950.0)	T ₁ (mag)	C-T ₁ (mag)	V _{hel} (km s ⁻¹)
4415	12 27 09.11	08 16 36.7	20.45	2.17	45000
2597	12 27 12.91	08 14 34.2	20.50	1.24	20000
2431	12 27 19.22	08 14 20.4	21.44	1.28	14800
1746	12 26 47.59	08 13 22.5	20.70	1.61	222
2430	12 27 03.46	08 14 20.4	21.45	1.75	-60
7790	12 26 47.97	08 20 34.7	19.74	1.41	11334
8113	12 27 06.93	08 21 02.1	20.88	1.33	10982
7569	12 27 35.79	08 20 16.3	21.25	1.44	10706
7039	12 27 43.90	08 19 34.2	21.21	1.70	34686
8062	12 27 30.61	08 20 58.8	19.97	1.18	83
9103	12 27 36.56	08 22 35.6	20.97	1.35	224
3900	12 27 16.98	08 16 00.0	21.04	1.89	10600
3217	12 27 36.55	08 15 16.3	21.05	1.29	8868
1922	12 27 37.08	08 13 36.7	21.16	1.60	32278
1024	12 27 14.18	08 12 12.5	20.99	1.11	200
1621	12 27 27.58	08 13 11.0	19.69	1.41	159
2935	12 27 40.19	08 14 57.6	19.87	1.06	133
1955	12 27 11.63	08 13 39.4	21.04	1.20	31000
8224	12 27 17.37	08 21 11.4	21.34	1.79	11700
6302	12 27 33.74	08 18 38.2	20.49	1.95	12000

¹ID from Geisler et al. (1996)

Sample	V_0 (km s^{-1})	V_{rot} (km s^{-1})	θ_0 (degrees)	V_{rot}^{max} (99%) (km s^{-1})
All clusters (N=144)	1018	69	181	< 130
Blue Clusters (N=93)	1059	101	177	< 200
Red Clusters (N=51)	940	15	180	< 75

Table 3: Results from non-linear fits of equation 1 to globular cluster samples taken from Table 1. The second column gives the mean velocity for each sample. The third column gives the least-squares fit to the rotation velocity and the fourth column gives the best-fit position angle. The final column gives the 99% upper limit on the rotational velocity.